Article
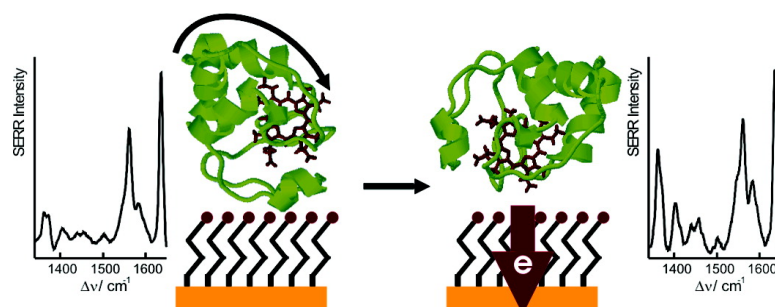
Direct Observation of the Gating Step in Protein Electron Transfer: Electric-Field-Controlled Protein Dynamics

Anja Kranich, Hoang Khoa Ly, Peter Hildebrandt, and Daniel H. Murgida

More About This Article

Additional resources and features associated with this article are available within the HTML version:

- Supporting Information
- Access to high resolution figures
- Links to articles and content related to this article
- Copyright permission to reproduce figures and/or text from this article

View the Full Text HTML

Direct Observation of the Gating Step in Protein Electron Transfer: Electric-Field-Controlled Protein Dynamics

Anja Kranich,[†] Hoang Khoa Ly,[†] Peter Hildebrandt,[†] and Daniel H. Murgida*,[‡]

Institut für Chemie, Technische Universität Berlin, Institut für Chemie, Str. des 17. Juni 135, D10623 Berlin, Germany, and Departamento de Química Inorgánica, Analítica y Química Física/INQUIMAE-CONICET, Facultad de Ciencias Exactas y Naturales, Universidad de Buenos Aires, Ciudad Universitaria, Pab. 2, piso 1, C1428EHA Buenos Aires, Argentina

Received March 6, 2008; E-mail: dhmurgida@qi.fcen.uba.ar

Abstract: Heterogeneous electron transfer of proteins at biomimetic interfaces is characterized by unusual distance dependences of the electron-transfer rates, whose origin has been elusive and controversial. Using a two-color, time-resolved, surface-enhanced resonance Raman spectroelectrochemical approach, we have been able to monitor simultaneously and in real time the structure, electron-transfer kinetics, and configurational fluctuations of cytochrome *c* electrostatically adsorbed to electrodes coated with self-assembled monolayers. Our results show that the overall electron-transfer kinetics is determined by protein dynamics rather than by tunnelling probabilities and that the protein dynamics in turn is controlled by the interfacial electric field. Implications for interprotein electron transfer at biological membranes are discussed.

Introduction

Protein dynamics has recently been recognized as a key factor in controlling or limiting inter- and intraprotein electron-transfer (ET) reactions in a number of cases, particularly in photosynthesis.[1–12] Because of the complexity of the systems, which impairs direct observations in most cases, conformational gating, configurational fluctuations, and rearrangement of protein complexes under reactive conditions are often inferred from indirect evidence. In this context, simplified model systems, such as proteins immobilized on electrodes coated with biocompatible films, can greatly contribute to a more-detailed understanding of the biophysical fundamentals, even though they unavoidably deviate from the true physiological conditions. Strategies for protein immobilization on electrodes are diverse, ranging from those trying to mimic biological ET complexes to others designed for studying basic aspects of protein ET or constructing bioelectronic devices. The most widely used electrode coatings are self-assembled monolayers (SAMs) of single or mixed alkanethiols containing ω functional groups that are chosen according to the protein's surface properties.[13] This approach has the specific advantage of facilitating the determination of ET rate constants as a function of distance simply by varying the chain length of the thiols. The geometric distance from the redox center of the adsorbed protein to the electrode is significant (>6 Å) even for the shortest possible alkanethiols. Therefore, one can anticipate a nonadiabatic ET mechanism with a characteristic exponential decay of the ET rate with increasing SAM thickness. However, in most of the systematic studies reported so far, "unusual" distance dependences have been found.[13–20] Specifically, for a number of proteins and different immobilization strategies, normal electron-tunneling decays have been observed for distances longer than 19 Å, but the measured rates became distance-independent for thinner spacers. The origin for this ubiquitous behavior has been elusive and controversial. For cytochrome *c* (Cyt) coordinatively bound to pyridine-terminated SAMs, a change of mechanism from the nonadiabatic to the adiabatic regime at a distance of 16 methylene groups has been proposed.[18,21] In contrast, for the same protein electrostatically adsorbed to carboxyl-terminated SAMs, the onset of change from "normal" to "unusual" distance

† Technische Universität Berlin.

‡ Universidad de Buenos Aires.

(1) Wang, H. Y.; Lin, S.; Allen, J. P.; Williams, J. C.; Blankert, S.; Laser, C.; Woodbury, N. W. *Science* **2007**, *316*, 747.

(2) Grove, T. Z.; Kostic, N. M. *J. Am. Chem. Soc.* **2003**, *125*, 10598.

(3) Jeuken, L. J. C. *Biochim. Biophys. Acta* **2003**, *1604*, 67.

(4) Kang, S. A.; Crane, B. R. *Proc. Natl. Acad. Sci. U.S.A.* **2005**, *102*, 15465.

(5) Lee, H. J.; Basran, J.; Scrutton, N. S. *Biochemistry* **1998**, *37*, 15513.

(6) Mei, H. K.; Wang, K. F.; Peffer, N.; Weatherly, G.; Cohen, D. S.; Miller, M.; Pielak, G.; Durham, B.; Millett, F. *Biochemistry* **1999**, *38*, 6846.

(7) Millett, F.; Durham, B. *Photosynth. Res.* **2004**, *82*, 1.

(8) Nocek, J. M.; Hatch, S. L.; Seifert, J. L.; Hunter, G. W.; Thomas, D. D.; Hoffman, B. M. *J. Am. Chem. Soc.* **2002**, *124*, 9404.

(9) Onuchic, J. N.; Kobayashi, C.; Miyashita, O.; Jennings, P.; Baldridge, K. K. *Philos. Trans. R. Soc. London* **2006**, *B361*, 1439.

(10) Zhuravleva, A. V.; Korzhnev, D. M.; Kupce, E.; Arseniev, A. S.; Billeter, M.; Orekhov, V. Y. *J. Mol. Biol.* **2004**, *342*, 1599.

(11) Chohan, K. K.; Jones, M.; Grossmann, J. G.; Frerman, F. E.; Scrutton, N. S.; Sutcliffe, M. J. *J. Biol. Chem.* **2001**, *276*, 34142.

(12) Davidson, V. L. *Acc. Chem. Res.* **2000**, *33*, 87.

(13) Murgida, D. H.; Hildebrandt, P. *Acc. Chem. Res.* **2004**, *37*, 854.

(14) Murgida, D. H.; Hildebrandt, P. *J. Am. Chem. Soc.* **2001**, *123*, 4062.

(15) Albrecht, T. Ph.D. Thesis, Technische Universität Berlin, 2003.

(16) Avila, A.; Gregory, B. W.; Niki, K.; Cotton, T. M. *J. Phys. Chem. B* **2000**, *104*, 2759.

(17) Chi, Q. J.; Zhang, J. D.; Andersen, J. E. T.; Ulstrup, J. *J. Phys. Chem. B* **2001**, *105*, 4669.

(18) Khoshtariya, D. E.; Wei, J. J.; Liu, H. Y.; Yue, H. J.; Waldeck, D. H. *J. Am. Chem. Soc.* **2003**, *125*, 7704.

(19) Fujita, K.; Nakamura, N.; Ohno, H.; Leigh, B. S.; Niki, K.; Gray, H. B.; Richards, J. H. *J. Am. Chem. Soc.* **2004**, *126*, 13954.

(20) Armstrong, F. A.; Barlow, N. L.; Burn, P. L.; Hoke, K. R.; Jeuken, L. J. C.; Shenton, C.; Webster, G. R. *Chem. Commun.* **2004**, 316.

(21) Yue, H.; Khoshtariya, D. E.; Waldeck, D. H.; Grochol, J.; Hildebrandt, P.; Murgida, D. H. *J. Phys. Chem. B* **2006**, *110*, 19906.

dependence has been observed at 10 methylene groups and rationalized either in terms of electric-field effects on protein reorganization[14,22] or as a gating mechanism in which the adsorbed Cyt must reorient from a thermodynamically stable but redox-inactive configuration to the orientation favorable for ET.[16,23] In all cases, the proposed mechanisms, although consistent with the experimental results, are based on rather indirect observations. Moreover, many of the arguments supporting one model also support the others.

Here we report a two-color, time-resolved (TR) surface-enhanced resonance Raman (SERR) spectroscopic study that, on the basis of direct observations, provides an unequivocal answer to this long-standing question. Specifically, we address the ET mechanism of Cyt electrostatically adsorbed on Ag electrodes coated with ω-carboxyl alkanethiols with various chain lengths.

Experimental Section

Chemicals. 8-Mercaptooctanoic acid (C_7) and 6-mercaptohexanoic acid (C_5) were purchased from Dojindo and 16-mercaptohexadecanoic acid (C_{15}) and 11-mercaptoundecanoic acid (C_{10}) from Sigma-Aldrich; all were used without further purification. Horse-heart Cyt was purchased from Sigma-Aldrich and purified by HPLC. The water used in all of the experiments was purified by a Millipore system, and its resistance was greater than 18 MΩ.

Electrode Modification. Silver ring electrodes were mechanically polished with 3M polishing films from 30 to 1 μm grade. After the electrodes were washed, they were subjected to oxidation–reduction cycles in 0.1 M KCl in order to create a surface-enhanced Raman (SER) active nanostructured surface. The electrodes were then incubated for 24 h in 1 mM solutions of the alkanethiols in ethanol, rinsed, and transferred to the spectroelectrochemical cell.

Surface-Enhanced Resonance Raman Spectroscopy. The spectroelectrochemical cell for SERR determinations has been described elsewhere.[24] Briefly, a Pt wire and a Ag/AgCl electrode were used as counter- and reference electrodes, respectively. All of the potentials cited in this work were referenced to the Ag/AgCl (3 M KCl) electrode. The working electrode was an 8 mm diameter by 2.5 mm height silver ring mounted on a shaft and rotated at 5 Hz to avoid laser-induced sample degradation.

The electrolyte solution [12.5 mM phosphate buffer (pH 7.0) containing 12.5 mM K_2SO_4] was bubbled with catalytically purified, oxygen-free argon prior to the measurements, and an overpressure of Ar was maintained during the experiments. Cyt from a stock solution was added to the electrochemical cell in an amount sufficient to form a 2–4 μM solution and allowed to incubate at room temperature for 15 min before the experiments were started.

SERR spectra were measured in the back-scattering geometry using a confocal microscope coupled to a single-stage spectrograph (Jobin Yvon LabRam 800 HR) equipped with a 2400 L/mm grating and a liquid nitrogen-cooled, back-illuminated CCD detector. Elastic scattering was rejected with Notch filters. The 413 nm line of a continuous-wave (cw) krypton ion laser (Coherent Innova 300c) or the 514 nm line of a cw argon ion laser (Coherent Innova 70c) was focused onto the surface of the rotating Ag electrode by means of a long-working-distance objective (20×, numerical aperture 0.35).

Typically, experiments were performed with a laser power of 1 mW (413 nm) or 12 mW (514 nm) at the sample. Effective acquisition times were 2–6 s. An increment of 0.57 cm^{-1} per data point and a spectral resolution of 2 cm^{-1} were used with 413 nm
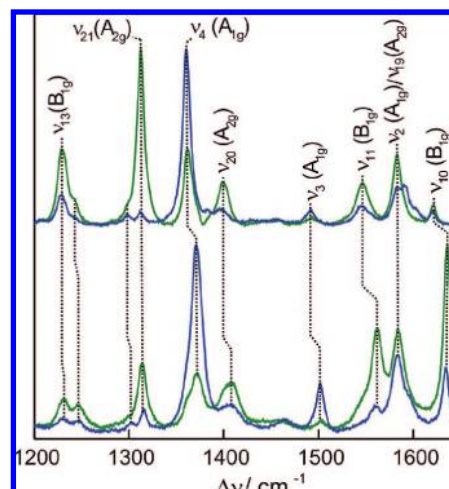
Figure 1. RR spectra of (top) ferrous and (bottom) ferric Cyt measured under Soret (blue lines; λ_{exc} = 413 nm) and Q-band (green lines; λ_{exc} = 514 nm) excitation. Bands are labeled according to ref 26.

excitation. Each experiment was repeated several times to ensure reproducibility.

In TR-SERR experiments, potential jumps of variable height and duration were applied to trigger the reaction. The SERR spectra were measured at variable delay times after each jump. Synchronization of potential jumps and measuring-laser pulses was achieved with a homemade four-channel pulse-delay generator. The measuring pulses were generated by passing the cw laser beam through two consecutive laser intensity modulators (Linos), which gave a total extinction of better than 1:50000 and a time response of 20 ns.

After background subtraction, the spectra were treated by single-band (514 nm) or component analysis[25] (413 nm) in which the spectra of the individual species were fitted to the measured spectra using in-house analysis software.

Results and Discussion

The resonance Raman (RR) spectrum of Cyt is dominated by the in-plane vibrational modes of the porphyrin chromophore. Preferential enhancement of the totally symmetric A_{1g} modes occurs upon Soret-band excitation, while the nontotally symmetric A_{2g}, B_{1g}, and B_{2g} modes gain intensity through Q-band excitation (Figure 1).[26]

In a SER experiment, i.e., one performed under off-resonance conditions, the individual components of the scattering tensor are modified in a manner that depends on the direction of the electric-field vector and the orientation of the heme plane. Assuming an idealized D_{4h} porphyrin symmetry, one can anticipate that the A_{1g} modes will experience preferential enhancement when the heme plane is parallel to the surface, while for a perpendicular orientation, the A_{1g}, A_{2g}, B_{1g}, and B_{2g} modes will all be enhanced.[27] Therefore, changing the orientation of the adsorbed protein is expected to lead to changes in the ratios of the intensities of modes of different symmetries, e.g., $I[\nu_{10}(B_{1g})]/I[\nu_4(A_{1g})]$ (hereafter labeled as $\nu_{10}(B_{1g})/\nu_4(A_{1g})$ for notational simplicity).

These selection rules are not applicable under strong resonance conditions, e.g., upon Soret-band excitation, partially

(22) Murgida, D. H.; Hildebrandt, P. *J. Phys. Chem. B* **2002**, *106*, 12814.
(23) Murgida, D. H.; Hildebrandt, P. *Phys. Chem. Chem. Phys.* **2005**, *7*, 3773.
(24) Murgida, D. H.; Hildebrandt, P. *J. Phys. Chem. B* **2001**, *105*, 1578.

(25) Dopner, S.; Hildebrandt, P.; Mauk, A. G.; Lenk, H.; Stempfle, W. *Spectrochim. Acta* **1996**, *52A*, 573.
(26) Hu, S. Z.; Morris, I. K.; Singh, J. P.; Smith, K. M.; Spiro, T. G. *J. Am. Chem. Soc.* **1993**, *115*, 12446.
(27) *Surface-Enhanced Raman Scattering: Physics and Applications*; Kneipp, K., Moskovits, M., Kneipp, H., Eds.; Springer: Berlin, 2006.

because of depolarization of the scattered radiation. However, a reasonable compromise between acceptable enhancement and qualitatively predictable selection rules can still be achieved upon Q-band excitation. In both cases, the high-frequency region $(1300-1700 \text{ cm}^{-1})$ of the SERR spectrum contains a number of bands that are particularly diagnostic for the redox state, spin, and coordination pattern of the heme iron.[13] Thus, an electrochemical experiment with SERR detection is able to provide simultaneous information on Faradaic processes and structural aspects of a heme protein immobilized on a SER active electrode in real time. Soret-band excitation measurements at 413 nm provide the highest sensitivity for monitoring the redox reaction (and, eventually, redox-linked structural changes) but are insensitive to protein reorientation. In contrast, Q-band excitation at 514 nm produces much weaker SERR spectra that are sensitive to the relative orientation of the heme plane and also to the redox state and the heme-pocket structure. Here we have employed two-color SERR spectroelectrochemistry to study the mechanism of heterogeneous ET of Cyt electrostatically adsorbed on nanostructured Ag electrodes coated with SAMs of ω-carboxyl alkanethiols with various chain lengths.

Stationary SERR measurements at 413 nm of Cyt adsorbed on COOH-terminated SAMs containing 5, 7, 10, and 15 methylene groups (C_5, C_7, C_{10}, and C_{15}, respectively) yield spectra which are essentially identical to the RR spectra of the native protein in solution in both the fully reduced and oxidized states. At intermediate potentials, the spectra can be quantitatively simulated using the RR spectra of native ferric and ferrous Cyt in solution as fixed components and only their relative contributions as adjustable parameters (not shown). The redox potentials of Cyt on the different coatings are very similar to the value for the native protein in solution, except for a small, distance-dependent shift that can be fully ascribed to the interfacial potential drop, as reported previously.[24] Thus, it is safe to conclude that the immobilized protein retains the native structure, at least at the level of the heme pocket. Redox potentials and surface coverage of Cyt on the different coatings have been reported elsewhere.[24]

In contrast, although the band widths and positions remain unchanged upon excitation at 514 nm, the intensity ratio $\nu_{10}(B_{1g})/\nu_4(A_{1g})$ shows a clear correlation with both the alkyl chain length of the SAM and the electrode potential (Figure 2). For a given SAM, the intensity ratio $\nu_{10}(B_{1g})/\nu_4(A_{1g})$ decreases when the potential is decreased, while for a fixed potential, this ratio decreases in a nearly exponential manner with increasing SAM thickness, tending to the value of the isotropic sample in solution at very long chain lengths. Both observations suggest that the local electric field at the SAM/Cyt interface actually controls the orientation. At constant ionic strength and pH, the electric field is determined by the charge of the electrode and the charge density at the plane of the carboxylate groups of the SAMs. The first quantity, in turn, depends on the difference between the actual electrode potential (E) and the potential of zero charge ($E_{pzc} \approx -1$ V for Ag), so the electric field diminishes as E approaches E_{pzc}. The second quantity is determined by the value of pK_a for the SAM, which increases with the chain length, and therefore, the electric field is weaker for longer tethers.[13] Thus, thinner SAMs or higher electrode potentials correspond to stronger electric fields.[23] The results indicate that stronger electric fields tend to more effectively align the dipole moment of the adsorbed protein, leading to a more perpendicular average orientation of the heme plane with respect to the electrode surface.
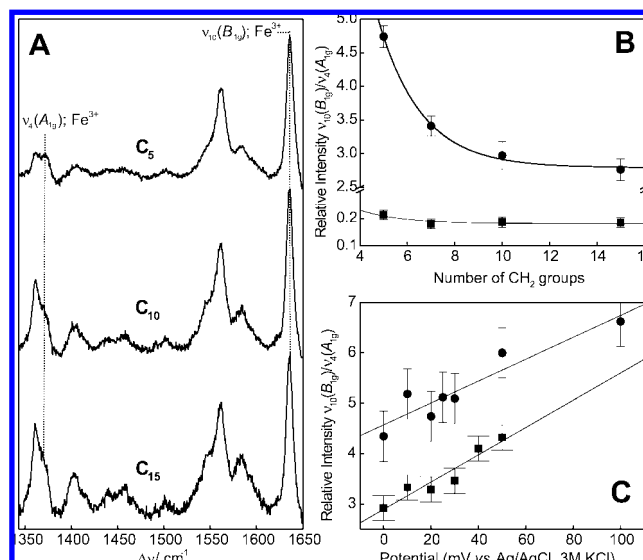

Figure 2. (A) SERR spectra of Cyt on electrodes coated with SAMs of various chain lengths (C_5, C_{10}, and C_{15}) measured at a fixed potential of 80 mV. (B) Chain-length dependence of the $\nu_{10}(B_{1g})/\nu_4(A_{1g})$ intensity ratio for ferric (●) and ferrous (■) Cyt measured at 0 mV. (C) Potential-dependence of the $\nu_{10}(B_{1g})/\nu_4(A_{1g})$ intensity ratio for ferric Cyt adsorbed on C_5 (●) and C_{10} (■) SAMs. All of the measurements were performed at pH 7.0 using 514 nm excitation.

The effect is quite remarkable for the oxidized protein, and qualitatively similar results are also observed for ferrous Cyt, although the magnitudes of the $\nu_{10}(B_{1g})/\nu_4(A_{1g})$ ratios are smaller (Figure 2B) and therefore subject to larger errors. It should be noted that the positions of the ν_{10} and ν_4 bands are very sensitive to the oxidation state of the heme iron and that orientation information for each redox state is extracted from the ratio of the intensities of these two bands using band-fit analysis. Therefore, ET and orientation/reorientation can be safely deconvoluted despite the differences in the SERR cross sections and $\nu_{10}(B_{1g})/\nu_4(A_{1g})$ ratios for the two species.

Upon application of a potential jump to an equilibrated sample, the orientation of the adsorbed ferric Cyt evolves toward the equilibrium value at the final potential, as directly monitored by TR-SERR with 514 nm excitation (Figure 3). The time scales for reorientation are strongly dependent on the chain lengths of the spacers and therefore on the electric field. For a C_5 SAM, the apparent rate constant for reorientation for a jump from 50 mV to −50 mV is $k_{reor}^{app} = 251 \text{ s}^{-1}$, while the apparent reduction rate constant measured by TR-SERR at 413 nm under otherwise identical conditions is $k_{red}^{app} = 220 \text{ s}^{-1}$. On the other hand, reorientation of ferric Cyt on a C_{15} SAM proceeds faster than the time resolution of the TR-SERR experiment ($k_{reor}^{app} > 6000$ s^{-1}), while the reduction rate constant is only $k_{red}^{app} = 0.43 \text{ s}^{-1}$ for a similar potential jump (Table 1).

For C_{10} SAMs, i.e., at the onset of the distance independence of k_{red}^{app}, reorientation and ET consistently remain kinetically separated for jumps to the redox potential but converge at higher overpotentials because the ET reaction accelerates while the rate of reorientation remains constant within experimental error (Figure 4). Thus, protein reorientation appears to be the rate-limiting event at short distances, while for long tethers, electron tunneling through the SAMs determines the measured rate.

Qualitatively, the results are consistent with a simple electrostatic model in which the charge density at the SAM surface determines the activation barrier for reorientation of the
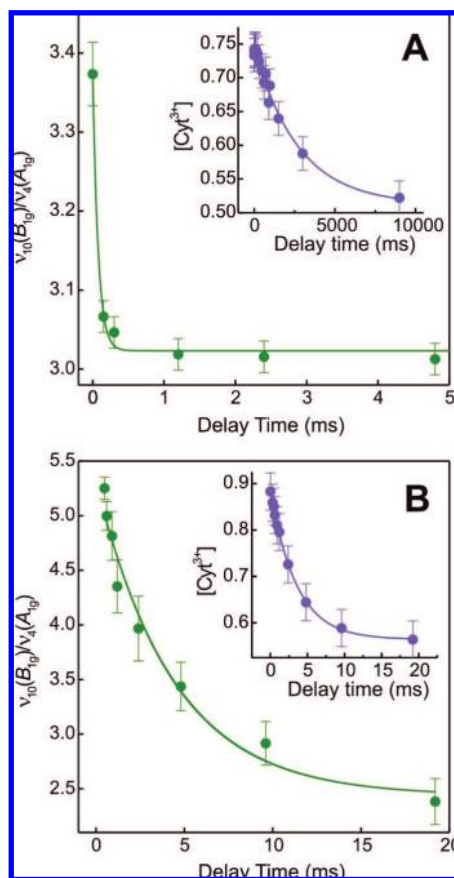
Figure 3. Time evolution of the $\nu_{10}(B_{1g})/\nu_4(A_{1g})$ intensity ratio for ferric Cyt adsorbed on (A) C_{15} and (B) C_5 SAMs after a potential jump from 50 to -50 mV. All of the measurements were performed at pH 7.0 using 514 nm excitation (green). The insets show the kinetics of Cyt reduction on the same SAMs as monitored by TR-SERR with 413 nm excitation (violet).
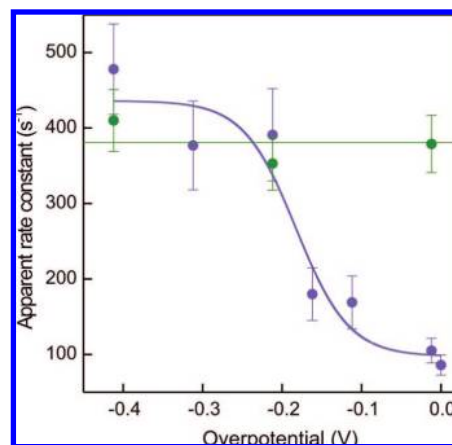
Table 1. Apparent Rate Constants for Reorientation and Reduction of Cyt Adsorbed on Different SAM-Coated Electrodes, As Determined by TR-SERR with 514 and 413 nm Excitation, Respectively[a]

| SAM	pH	k_{reor}^{app} (s^{-1})	k_{red}^{app} (s^{-1})
C_5	6.0	370 ± 35	340 ± 25
	7.0	251 ± 25	220 ± 20
	7.8	160 ± 16	180 ± 10
C_{10}	7.0	379 ± 30	105 ± 12
C_{15}	7.0	>6000	0.43 ± 0.05

[a] All of the values refer to potential jumps from 50 to -50 mV, except that for C_{10}, which refers to a jump from 40 to 0 mV.

electrostatic complex above the threshold of thermal energy. In agreement with this conclusion, we observed that for Cyt adsorbed on a C_5 SAM, the apparent rate constant for reorientation increases with decreasing pH: $k_{reor}^{app} = 160$, 250, and 370 s^{-1} at pH 7.8, 7.0, and 6.0, respectively (Figure 5 and Table 1). Within experimental error, the apparent rate constants for ET are very similar to those for reorientation and exhibit similar pH dependence.

Within this pH range, the formal potential of Cyt remains constant within experimental error, and no acidic or alkaline transitions were observed spectroscopically. On the other hand, a change in pH affects protonation of the SAM more dramatically than that of the protein, so the acceleration of the reaction at lower pH can also be understood in terms of a weaker electric field. Furthermore, for the same system at pH 7, a 20% increase

Figure 4. Apparent rate constants for ET (violet) and reorientation (green) for ferric Cyt adsorbed on a C_{10} SAM, measured with 413 and 514 nm excitation, respectively, at pH 7.0.
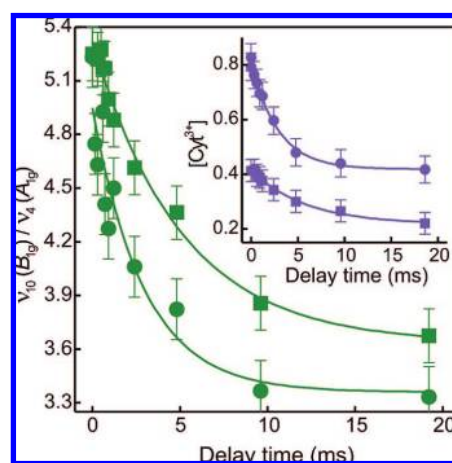
Figure 5. Time evolution of the $\nu_{10}(B_{1g})/\nu_4(A_{1g})$ intensity ratio for ferric Cyt adsorbed on a C_5 SAM, as determined by TR-SERR with 514 nm excitation (green) at pH 6 (●) and 7.8 (■) for potential jumps from 50 to -50 mV. The inset shows the kinetics of Cyt reduction monitored by TR-SERR with 413 nm excitation (violet) under otherwise identical conditions. The violet curves have been vertically displaced for better visualization.

of the solution viscosity (accomplished by addition of sucrose) reduces both apparent rate constants by a factor of 2 (see the Supporting Information).

Conclusions

The SERR spectroelectrochemical experiments reported here show that the average orientation of Cyt in electrostatic complexes with SAM-coated electrodes is dependent on the electrode potential and the charge density of the coating. Application of a potential jump triggers reorientation of the protein relative to the electrode surface in addition to net ET. Reorientation is very fast for thick SAMs, i.e., at low electric fields, but slows down dramatically and becomes rate-limiting at short distances. Thus, while the measured ET rates are determined by electron tunneling probabilities at long distances, the reaction is controlled by protein dynamics for thin SAMs.

It should be noted that the description of the interfacial electric field adopted here tacitly assumes a highly ordered SAM. It is known, however, that thinner SAMs are less ordered than thicker ones. This microscopic disorder is reflected in the lower pK_a values reported for thinner films, and therefore, it is empirically included in the electrostatic model at least partially.[13,23,28] Other

effects of the decreased order in thin SAMs cannot be excluded, but the consistency of the results in terms of the distance, potential, and pH dependences of orientation/reorientation of Cyt indicate that such effects are not dominant and at most could affect only the rate-constant magnitudes but not the observed trends.

To the best of our knowledge, this is the first time that structure, ET, and configurational dynamics of a redox-active molecular film have been simultaneously and directly monitored.

In principle, our results are compatible with a minimal two-state kinetic model in which one state is a thermodynamically stable, redox-inactive orientation and the other is a single redox-active orientation, except that the binding energies and reorientation rates are not distance- and redox-state-independent as originally proposed by Avila et al.[16] Very recently, Araci et al.[29] showed that the heterogeneous ET kinetics of Cyt directly adsorbed on indium–tin oxide (ITO) electrodes can be rationalized in terms of two rate constants, each representing one of two differently oriented subpopulations of Cyt in the film. Although the surface properties of ITO are different, these results are in clear contradiction with the model of Avila et al.

The picture emerging from the present studies is that local electric fields determine both the mean orientation and the mobility of Cyt in electrostatic complexes. Thus, the measured ET rates represent a convolution of dynamic sampling of the surface in search of a favorable ET pathway and electron tunneling probabilities at each configuration.

Electric-field control of the overall ET rates via modulation of protein dynamics seems to be a widespread phenomenon in bioelectrochemistry and bioelectronics. One can envisage similar effects controlling interprotein ET in vivo, such as in photosynthesis and respiratory chains. In both cases, the cascade of ET reactions is coupled to proton translocation across the membrane, generating a gradient that drives ATP synthesis. This implies a variable electric field during turnover, affecting the sampling rate of optimal ET pathways in transient and long-lived complexes between membrane-bound proteins and soluble electron carriers (e.g., Cyt-oxidase and Cyt). Such an effect might constitute the basis for a feedback regulating mechanism.

Supporting Information Available: TR-SERR spectra and kinetic traces for various viscosities. This material is available free of charge via the Internet at http://pubs.acs.org.

JA8016895

(28) Murgida, D. H.; Hildebrandt, P. *Chem. Soc. Rev.* **2008**, *37*, 937.
(29) Araci, Z. O.; Runge, A. F.; Doherty, W. J., III; Saavedra, S. S. *J. Am. Chem. Soc.* **2008**, *130*, 1572.